

# Büttiker Probe Based Modeling of TDDB: Application to Dielectric Breakdown in MTJs and MOS Devices

Ahmed Kamal Reza, Mohammad Khaled Hassan and Kaushik Roy

**Abstract**— Dielectric layers are gradually being downscaled in different electronic devices like MOSFETs and Magnetic Tunnel Junctions (MTJ) with shrinking device sizes. As a result, time dependent dielectric breakdown (TDDB) has become a major issue in such devices. In this paper we propose a generalized way of modeling the stress induced leakage current (SILC) and post breakdown current (PBC) due to time dependent wear-out of the dielectric layer. We model the traps formed in dielectric layer using Büttiker probe [1] and incorporate the Büttiker probe self-energies in standard self-consistent Non-Equilibrium Green's Function (NEGF) formalism [2] in order to determine SILC and PBC. In addition, we have shown the impact of break down in the dielectric layer on the spin current and spin filtering characteristics of an MTJ. The proposed model is generic in nature. It can be extended from MTJs and conventional CMOS technology to any other devices with any type of single and multiple layers of dielectric material(s).

**Index Terms**— Magnetic tunnel junction (MTJ), Time dependent Dielectric Breakdown (TDDB), Spin Current Degradation, Non-equilibrium Green's function (NEGF), Büttiker probe, Stress Induced Leakage Current (SILC), Soft Breakdown, Hard Breakdown.

## I. INTRODUCTION

EXTENSIVE research is currently being done on spin based memory, logic and neuromorphic computing devices and circuits. Today, MTJs are becoming an indispensable part in almost all spin-based systems. In order to achieve better write current, researchers are now fabricating MTJs with  $\sim 1\text{nm}$  thick MgO layer in between the fixed and free ferromagnetic layers [3]. As a result, the voltage applied across these thin oxide layers can generate a tremendous amount of stress electric field (on the order of  $10^8\text{-}10^9\text{ V/m}$ ). Gradually traps start forming in the dielectric layer that eventually lead to the formation of percolation paths. When electron is captured by a trap, the spin orientation of that electron is randomized. As a result, the spin filtering efficiency of the MTJ starts degrading over time, eventually causing functional failures.

Post-breakdown I-V characteristics primarily depends on the type dielectric breakdown. Sometimes the post-breakdown current-voltage characteristic is vastly different from its no-breakdown counterpart and follows Ohm's law [4]. Then the dielectric is said to have experienced a hard breakdown. On the other hand, soft dielectric breakdown is characterized by a power law dependence between post-breakdown current and corresponding voltage [4]. But the increase in post breakdown current is small compared to no breakdown current. Over the past decade a lot of research [4-9] focused on the breakdown characteristics/models of dielectric layers, especially for MOS devices. These models are mainly analytical in nature and can predict the breakdown behavior such as, post break down I-V characteristics and the time to failure. However, the analytical

models are not sufficient to predict the spin current degradation through MTJ due to dielectric breakdown. This is because the ferromagnetic layers can be either in parallel or anti parallel states and the tunneling ferromagnetic resistance varies with the corresponding magnetization orientation. In addition, different ferromagnetic layers can have different exchange coupling energy and different band structures that play a significant role in determining the post breakdown MTJ characteristics.

In this paper we propose a unified model for predicting the I-V characteristics of the dielectric layer due to formation of traps at different positions and at different energy levels. In the next section we discuss our simulation framework and show how Büttiker probe [1] can be used to model the traps. We have shown that our model can predict the behavior of the dielectric layer after both soft and hard breakdowns. We have verified our model with the experimental results of post breakdown I-V characteristics of both conventional MOSFETs (with both single  $\text{SiO}_2$  layer and  $\text{HfSiON/SiO}_2$  multilayer as gate oxide) and MTJ. We also used NEGF formalism to calculate the spin current for both parallel and antiparallel states in order to determine the degradation of the tunneling magnetoresistance (TMR) due to the TDDB effect in MgO layer in MTJs.

## II. PROPOSED SIMULATION FRAMEWORK USING BÜTTIKER PROBE

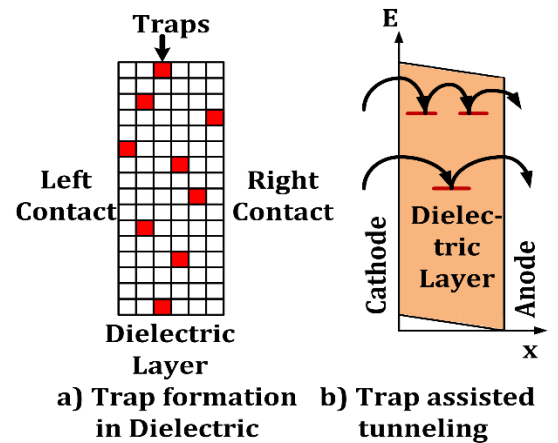


Fig.1.: Schematic diagram of trap position (a) Physical positions of trap (b) Energy level positions of traps.

In this section we first discuss some of the major attributes of trap assisted tunneling. First of all, the capture cross section of a trap in a particular dielectric depends on its position in the energy level [10]. A mid-bandgap trap has a relatively bigger capture cross-section than the ones near the conduction band edge or in the conduction band [11]. Researchers usually measure it experimentally and in this paper we will use those experimentally measured values in our analyses. Another

important thing to consider is the physical position of the trap. The physical position of a trap determines the distance that a carrier has to tunnel before being captured by the trap. Cell based standard percolation model [12] can be used to determine whether it is a surface trap or a bulk trap.

In figure 1 we have shown a schematic diagram of both the physical position and energy level of traps for an example dielectric. A major characteristic of trap assisted tunneling is the dephasing of the electron or hole when captured by a trap. Therefore, the tunneling probability and the dephasing of carrier need to be modeled simultaneously. We model the traps using Büttiker probes.

#### A. Modelling traps with Büttiker probe

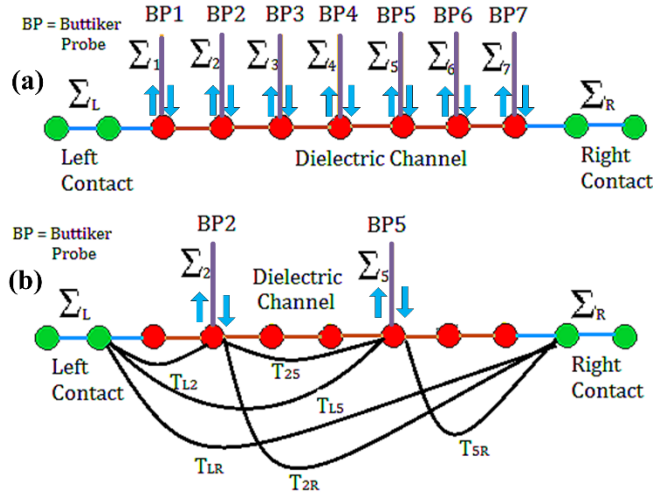


Fig.(2a). Concept of Büttiker probe. A virtual contact is attached to grid points where trap is generated. These additional contacts are treated with a self-energy, like the real contacts. (2b) Assuming traps are formed at grid position 2 and 5, we have attached Büttiker probe to these positions. All possible tunneling paths are shown with corresponding tunneling transmission probability

In Fig. 2(a) explains the concept of Büttiker probes. Büttiker probes are virtual probes that can be inserted at the grid positions where traps are generated. In the same figure, there are two more contacts attached to the dielectric channel in addition to the Büttiker probes. In case of MTJ the left and right contacts are the two ferromagnetic layers, i.e., the fixed layer and the free layer [13]. For MOSFETs, these two contacts are the top metal or polysilicon layer and the bottom channel or the substrate layer. In Fig. 2(a), as the channel is an insulator, the electrons mainly tunnel through the dielectric layer from one contact to the other. We have assumed that there are no pre-existing traps in the dielectric layer and after application of a voltage across the dielectric layer, the Fermi functions at left and right contacts are  $f_L(E)$  and  $f_R(E)$ , respectively. The current density can be written as [14].

$$J = \frac{1}{q} \int G(E) (f_R - f_L) dE \quad (1)$$

Here  $G(E)$  is the conductance and  $q$  is the electron charge.  $G(E)$  is defined as [3],  $G(E) = \frac{q^2}{h} T(E)$  where  $T(E)$  is the transmission probability. The transmission probability depends on the retarded Green's function of the system and the self-energy matrices of the contacts. The retarded Green's function

can be written as follows [14]

$$\mathbf{G}^R = [\mathbf{E}\mathbf{I} - \mathbf{H} - \boldsymbol{\Sigma}_L - \boldsymbol{\Sigma}_R]^{-1} \quad (2)$$

where,  $\boldsymbol{\Sigma}_L$  and  $\boldsymbol{\Sigma}_R$  are the self-energy matrices of the left and right contacts, respectively.

Therefore, the transmission probability between the left and right contact can be represented as [14]

$$T_{LR} = \text{Trace} [\boldsymbol{\Gamma}_L \mathbf{G}^R \boldsymbol{\Gamma}_R \mathbf{G}^A] \quad (3)$$

Where,  $\mathbf{G}^A$  is the complex conjugate matrix of  $\mathbf{G}^R$ . Here  $\boldsymbol{\Gamma}_L$  and  $\boldsymbol{\Gamma}_R$  are two quantities defined as [14]  $\boldsymbol{\Gamma}_L = i[\boldsymbol{\Sigma}_L - \boldsymbol{\Sigma}_L^\dagger]$  and  $\boldsymbol{\Gamma}_R = i[\boldsymbol{\Sigma}_R - \boldsymbol{\Sigma}_R^\dagger]$ .  $\boldsymbol{\Sigma}_L^\dagger$  and  $\boldsymbol{\Sigma}_R^\dagger$  are the complex conjugate matrices of  $\boldsymbol{\Sigma}_L$  and  $\boldsymbol{\Sigma}_R$ , respectively.  $\boldsymbol{\Gamma}$  is a matrix that physically represents how easily carriers can get in or get out of a contact [14].

Let us assume that traps are formed at grid position 2 and 5 (fig. 2b). For modelling these two traps, we need to attach two Büttiker probes at those two grid points as shown in figure 2b. These probes absorb carriers, dephase them, and inject them back to the channel. As a result, there is no net current through these probes i.e., the current conservation law is followed.

Note that the electrons have multiple paths for going from the left contact to the right contact. Electrons can be captured by the trap at grid point 2, then recaptured by the trap at grid point 5 and finally escape through the right contact (fig 2b). Again electrons can tunnel from left contact to either traps at grid position 2 or grid position 5 and then tunnel to the right contact (fig 2b). Moreover, they can directly tunnel from left contact to right contact. Now let us consider the first trap assisted tunneling path. The corresponding tunneling transmission probabilities are  $T_{L2}$ ,  $T_{25}$  and  $T_{5R}$ . These tunneling paths are in series connection with one another and the tunneling transmission probability is proportional to conductance. Therefore, the total tunneling transmission probability of this path,  $T_{L25R}$  can be written as

$$\frac{1}{T_{L25R}} = \frac{1}{T_{L2}} + \frac{1}{T_{25}} + \frac{1}{T_{5R}} \quad (4)$$

Where  $T_{L2} = \text{Trace} [\boldsymbol{\Gamma}_L \mathbf{G}^R \boldsymbol{\Gamma}_2 \mathbf{G}^A]$ ,  $T_{25} = \text{Trace} [\boldsymbol{\Gamma}_2 \mathbf{G}^R \boldsymbol{\Gamma}_5 \mathbf{G}^A]$  and  $T_{5R} = \text{Trace} [\boldsymbol{\Gamma}_5 \mathbf{G}^R \boldsymbol{\Gamma}_R \mathbf{G}^A]$ . Again if  $\boldsymbol{\Sigma}_2$  and  $\boldsymbol{\Sigma}_5$  are the self-energy matrices of the Büttiker probes attached at grid positions 2 and 5, then  $\boldsymbol{\Gamma}_2 = i[\boldsymbol{\Sigma}_2 - \boldsymbol{\Sigma}_2^\dagger]$  and  $\boldsymbol{\Gamma}_5 = i[\boldsymbol{\Sigma}_5 - \boldsymbol{\Sigma}_5^\dagger]$ . In simple effective mass simulation the we have calculated the self-energy matrix of Büttiker probe as follows

$$\boldsymbol{\Sigma}_{\text{Büttiker}} = \begin{bmatrix} (-t_{de} - qV_{eff}^\alpha) \exp(ika) & 0 \\ 0 & (-t_{de} - qV_{eff}^\alpha) \exp(ika) \end{bmatrix} \quad (5)$$

Here  $a$  is the grid mesh size and  $t_{ox}$  is defined as  $t_{de} = \frac{\hbar^2}{2m_{de}} a^2$  where  $m_{de}$  is the electron effective mass in the dielectric.  $V_{eff}$  is the effective voltage at the trap position. When a voltage is applied across a dielectric layer the whole voltage can be assumed to appear and be uniformly distributed across that layer. Hence the effective voltage at different trap positions is different. Effective voltage has got a power factor  $\alpha$  over it. The power factor appears because the current due to soft breakdown of dielectric layer exhibits power law dependence on the corresponding voltage. Hence for soft dielectric breakdown,  $\alpha$  is greater than 1. But when there is a hard breakdown  $\alpha$  is equal to 1. Therefore, when a percolation path is formed, the type of breakdown needs to be determined first and the  $\alpha$  factor is tuned accordingly. Also the value of  $\alpha$

depends on the dielectric material and the capture cross section of the trap. For larger capture cross section  $\alpha$  is larger. In equation (4)  $k$  is the wave vector defined as

$$k = \cos^{-1}\left(1 - \frac{E - qV_{eff}^\alpha + \xi i}{2t_{de}}\right) \quad (6)$$

$\xi$  is a very small arbitrary energy. One thing worth mentioning is that except hard breakdown we should not add the self-energy matrices of Büttiker probes to the system Green's function. This is because Büttiker probes are artificial probes introduced for modelling. They are not the part of actual physical system. Hence, introduction of Büttiker probes should not disturb the system Green's function. But when there is a hard breakdown, the channel's transport characteristic is changed from tunneling to Ohmic conduction. Hence the system's Green's function is modified according to the following equation

$$\mathbf{G}^R = [\mathbf{E}\mathbf{I} - \mathbf{H} - \boldsymbol{\Sigma}_L - \boldsymbol{\Sigma}_R - \boldsymbol{\Sigma}_1 - \boldsymbol{\Sigma}_2 - \dots - \boldsymbol{\Sigma}_n]^{-1} \quad (7)$$

Here  $\boldsymbol{\Sigma}_1, \boldsymbol{\Sigma}_2, \dots, \boldsymbol{\Sigma}_n$  are the self-energy matrices of the Büttiker probes attached along the channel.

Note from figure 2(b) let us consider other trap assisted tunneling paths. Electrons can be captured first by the trap at grid position 2 and then it can tunnel to the right contact. In this case the tunneling transmission coefficient

$$\frac{1}{T_{L2R}} = \frac{1}{T_{L2}} + \frac{1}{T_{2R}} \quad (8)$$

where  $T_{2R} = \text{Trace}[\boldsymbol{\Gamma}_2 \mathbf{G}^R \boldsymbol{\Gamma}_R \mathbf{G}^A]$ .

Similarly, as stated earlier, electron can travel from left contact to the trap at grid position 5 and then to right contact (fig 2b). Hence, the tunneling transmission coefficient

$$\frac{1}{T_{L5R}} = \frac{1}{T_{L5}} + \frac{1}{T_{5R}} \quad (9)$$

Here  $T_{L5} = \text{Trace}[\boldsymbol{\Gamma}_L \mathbf{G}^R \boldsymbol{\Gamma}_5 \mathbf{G}^A]$ . Note, the electron can tunnel directly from left contact to right contact. Hence, there are a total 4 paths for electrons for electrons to tunnel from left to right contact (fig 2b). As all these paths are parallel, the overall tunneling transmission coefficient

$$T_{all} = T_{L25R} + T_{L2R} + T_{L5R} + T_{LR} \quad (10)$$

The total tunneling current can be expressed as

$$J = \frac{q}{h} \int T_{all} (f_R - f_L) dE. \quad (11)$$

Now if the traps line up a percolation path is formed. Post breakdown I-V characteristic can be modelled in the same way by attaching Büttiker probe to all the grid points along the thickness. While using this method for MOS devices, channel will act as the right contact in fig 1. Therefore, the potential profile in the channel region should be carefully modelled and probe mapped into system Hamiltonian. Especially if drain voltage is applied then the potential profile will be asymmetric near source and drain region. Then we can divide the gate into small areas in which the potential profile can be assumed constant. Then current through each area can be added up to get total gate tunneling current. Also we need to consider the effect of flat band voltage and charge accumulation profile in channel before and after inversion. Also if the dielectric layer consists of multiple layer, potential profile in each layer should be determined carefully and included in the Hamiltonian accordingly.

Now the spin current density is defined between two successive

lattice point as [15] [16]

$$J_s = \frac{2\pi}{i\hbar} \int \text{Real}[\text{Trace}(\mathbf{S} \cdot (\mathbf{H}\mathbf{G}^n - \mathbf{G}^n\mathbf{H}))] dE. \quad (12)$$

Where,  $\mathbf{H}$  is the system Hamiltonian and  $\mathbf{S}$  is Pauli matrix. Let the fixed layer and free is pointing at Z direction and we are interested in calculating the z-oriented spin current.

It can be shown that the above equation can be written as

$$J_s = \frac{q}{h} \int \text{Real}(\text{Trace}(\mathbf{S} \cdot (\boldsymbol{\Gamma}_L \mathbf{G}^R \boldsymbol{\Gamma}_R \mathbf{G}^A))) (f_R - f_L) dE. \quad (13)$$

One important thing is that the magnetic contact self-energy contains the exchange splitting energy,  $\Delta$ . But trap's electron capturing capability is independent of spin. Therefore, Büttiker probe self-energy matrix does not contain  $\Delta$ .

### III. RESULTS AND DISCUSSION

In the dielectrics, stress induced traps due to high electric field eventually lead to formation of percolation paths. In this section, our proposed model is applied to calculate the stress-induced leakage current (SILC) due to the formation of multiple traps in HfSiON. It is followed by calculation of soft breakdown (SBD) and hard breakdown (HBD) current in SiO<sub>2</sub>. The results are in close agreement with the experimental data. Then we consider the formation of percolation paths in MgO. We apply our simulation framework to calculate the post breakdown I-V characteristics and compare against experimental results. We have also calculated the TMR degradation in MTJ due to formation of percolation paths in MgO. Then we predict the lifetime of the MTJ based on our calculation.

#### A. Stress Induced Leakage Current (SILC)

The extensive use of amorphous dielectrics in electronic devices has made it a very important problem to analyze the effect of traps and point defects both in the bulk and on the surface of dielectric. Traps can be either pre-existing or they can form over time due to stress. Here we analyze the traps formed due to stress from high electric field. We have initially considered defect free 1.4nm HfSiON layer and 0.8nm SiO<sub>2</sub> interface layer (IL) and matched the I-V characteristic with experimental data from [17]. Simulation parameters are listed in table I. Then we assume a trap density of  $1.5 \times 10^{19}/\text{m}^3$  at the HfSiON and SiO<sub>2</sub> interface and calculated the SILC. The work presented in [17] does not provide any information regarding the number of traps or their locations. As the probability of trap formation is higher near high- $\kappa$  dielectric and SiO<sub>2</sub> IL [18], we have assumed that traps are formed near the interface. Then we have varied the number of traps to see when calculated SILC is matching better with experiment. Thus with Büttiker probe method we can calculate the stress induced trap density. Also mismatch in initial gate current-gate voltage characteristic from NEGF formalism with the experiment indicates the presence of pre-existing traps. Then by using the Büttiker probes in NEGF formalism and matching the initial Ig-Vg characteristic, we can determine the pre-existing trap density in the structure.

#### B. SiO<sub>2</sub> Soft Breakdown

It has been experimentally observed that the SBD in dielectrics is characteristically different from the HBD [4]. In thinner oxides, post breakdown I-V characteristics shows comparatively smaller change from no breakdown characteristics and follows power law. Soft breakdown can be

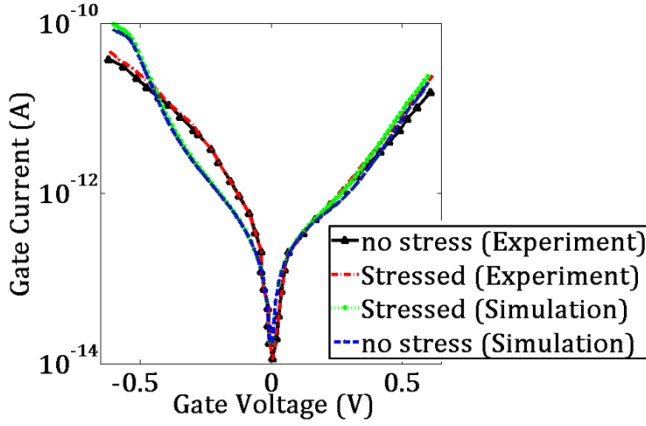


Fig. 3. Pre and post stress induced leakage current for 1.4 nm HfSiON and 0.8nm SiO<sub>2</sub> IL (both experiment [17] and simulation).

modeled with our proposed Büttiker probe by attaching probe to all grid points along the thickness. Now if we tune the power factor  $\alpha$  of equation (5) we can get excellent matching of post breakdown I-V characteristics. In [19] the post soft breakdown I-V characteristic in a MOS capacitor (Poly-Si/SiO<sub>2</sub>/Si system) have been experimentally demonstrated. After calibration we have found that the Büttiker probe power factor  $\alpha = 1.7$  and we have seen excellent match of our simulation result with experimental observation (shown in figure 4(a)). Here one thing worth mentioning is that the power factor  $\alpha$  depends on the capture cross section. As mentioned earlier, capture cross section depends on the energy level of the traps and traps at the percolation path can form at different energy levels. Therefore,  $\alpha$  can be different for different Büttiker probes. Simulation parameters are listed in table I.

### C. SiO<sub>2</sub> Hard Breakdown

Hard breakdowns mainly occur in thick dielectrics [24]. This is because in thick dielectrics the gate voltage is very high. Hard breakdown can be easily separated from soft breakdown by the huge change in PBD current and Ohmic nature of the PBD I-V characteristics. For this case the power factor  $\alpha$  in equation 5 will be 1. In [4] post hard breakdown I-V characteristic is shown for a MOS capacitor with 2.2nm thick SiO<sub>2</sub>. In figure 5 we have shown both the experimental and simulation data before and after hard breakdown. It is evident that after hard breakdown gate leakage current increases by several orders of magnitude but the increase of current with voltage is almost linear.

### D. MgO Soft Breakdown

MgO is a mid- $\kappa$  dielectric with a low Weibull slope [25]. Therefore, from reliability point of view MgO layer has a high lifetime. Furthermore, it has gained popularity due to its excellent spin current filtering capacity. Hence it has become the prime choice for fabricating MTJ. In [26], a post soft breakdown I-V characteristic of 1nm thick MgO in an MTJ is reported. The MTJ stack is comprised of CoFeB/MgO/CoFeB. It was observed in [26] that the activation temperature of MgO is quite high (265°C to 400°C). Therefore, although the bulk trap

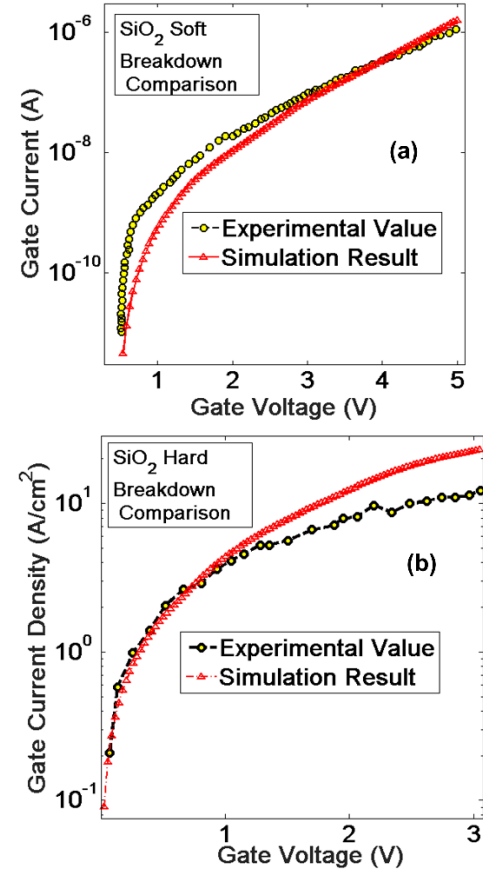


Fig. 4(a). Post soft breakdown current for 1.7 nm SiO<sub>2</sub> (both experiment [23] and simulation). 4(b). Post hard breakdown current for 2.2 nm SiO<sub>2</sub> (both experiment [24] and simulation).

has large capture cross section [27], in a very thin MgO layer, the trap energy levels are distributed near conduction band edge. As a result, the trap capturing cross section will be much smaller than the bulk value. For a soft breakdown calibration with experiment [26] as shown in figure 5 experimental and simulation data of post soft breakdown I-V characteristics is shown and, the value of  $\alpha$  is set to be equal to 9. Breakdown in MgO layer has a significant impact on the MTJ characteristics. In figure 6a we have shown the parallel and antiparallel tunneling magnetoresistance ( $R_p$  and  $R_{AP}$  respectively) of an CoFeB-MgO-CoFeB MTJ with 1nm thick MgO layer (same structure as shown in ref [27]). We can see  $R_{AP}$  is decreasing at much faster rate than  $R_p$ . This is because  $R_p$  is mainly dominated by the exchange splitting energy,  $\Delta$  of the magnetic contacts (shown in fig. 7a). For parallel configuration, huge exchange coupling allows the majority spin to tunnel easily and formation of a percolation path does not affect this process significantly. But for the antiparallel configuration this exchange splitting energy opposes the spin tunneling and therefore a percolation path significantly decreases the  $R_{AP}$ .



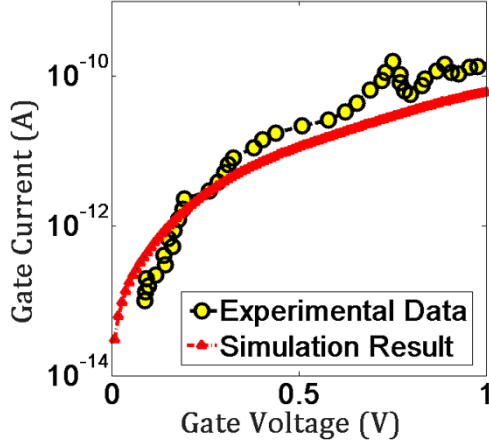


Fig. 5: Post soft breakdown current voltage characteristics from experiment [26] and from our simulation framework

TABLE I  
PARAMETERS USED IN BÜTTIKER PROBE SIMULATION

Parameter Name	Value
Grid mesh size	0.1 nm
CoFeB effective mass	0.38 [28]
MgO tunneling effective mass	0.16 [29]
TiN effective mass	1.1 [30]
Si effective mass	0.26
SiO <sub>2</sub> tunneling effective mass	0.42 [31]
HfSiON tunneling effective mass	0.03 [32]
Temperature	300 k
HfSiON bandgap	5.32 eV
HfSiON electron affinity	2.95 eV
TiN work function	4.4 eV
SiO <sub>2</sub> bandgap	9 eV
SiO <sub>2</sub> electron affinity	0.95 eV
Si electron affinity	4.05 eV
Si-SiO <sub>2</sub> barrier height	3.1 eV
TiN-HfSiON barrier height	1.45 eV
CoFeB-MgO barrier height	0.76 eV
CoFeB-MgO Fermi level	2.25 eV
Si-SiO <sub>2</sub> Fermi level	3.9 eV

Traps inside the MgO layer helps tunneling irrespective of electron spin. When an electron is captured by a trap its spin properties get randomized. The spin wave function of an electron in a trap can be represented as

$$|\psi_s\rangle = a_{z+}|u_{z+}\rangle + a_{z-}|d_{z-}\rangle$$

Here  $a_{z+}|a_{z+}^*$ ,  $|u_{z+}\rangle$ ,  $a_{z-}|a_{z-}^*$  and  $|d_{z+}\rangle$  represents the spin polarization probability and spin basis vector (spinors) along +z and -z axis respectively. These two spinors can represent spin pointing at any direction [28]. In a trap it can be assumed that these two probabilities are equal i.e.,  $a_{z+}|a_{z+}^* = a_{z-}|a_{z-}^*$ . Therefore, the spin filtering efficiency of the MgO layer is going down after the formation of traps and percolation paths.

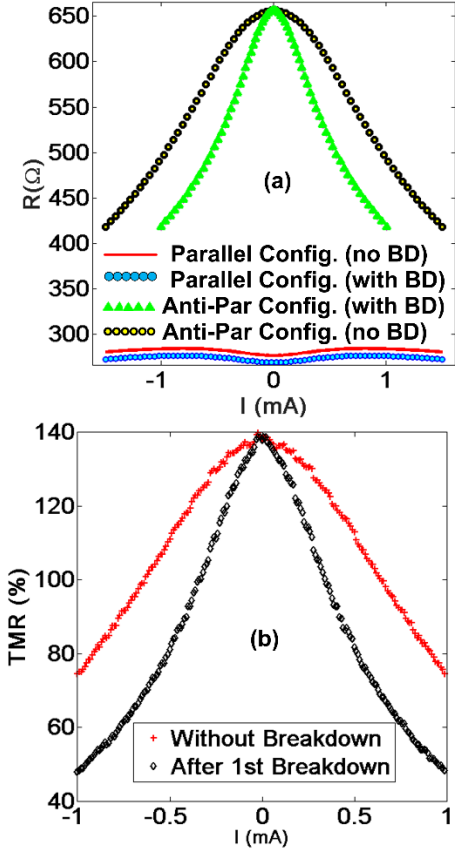


Fig.6(a): Pre and post breakdown (bd) parallel and antiparallel resistance (b) Change in %TMR before and after breakdown (bd).

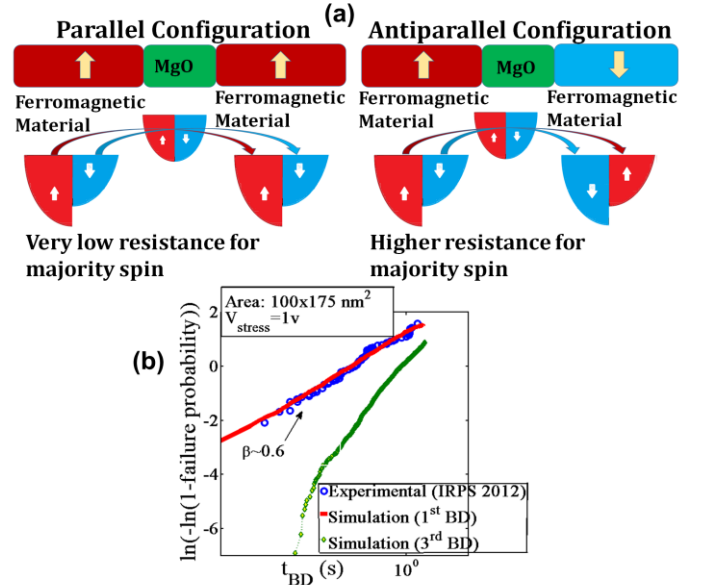


Fig.7.(a): Schematic band diagram of CoFeB-MgO-CoFeB MTJ. (b) Weibull plot of MgO for 1<sup>st</sup> and 3<sup>rd</sup> breakdown

From fig 7(a) we can see that if the MTJ is operated at 1mA current (operating voltage  $V \sim 0.5V$ ) then every soft breakdown will cause about 25% degradation in percentage TMR (fig 6b). Therefore, after 3-4 soft breakdowns in the MgO layer, the MTJ

will not be functional. Now using a 3D cell percolation model we have calibrated the Weibull plot with experimental data [29]. From the Weibull plot (fig. 7(b)), using standard area scaling [30] we can see that 1% MTJ in 10000 sample MTJs will have 3<sup>rd</sup> soft breakdown in 16 years.

#### IV. CONCLUSION

In this work, we have presented a Büttiker probe based post breakdown current model for dielectric materials. The method is flexible, can be applied to a wide range of dielectric materials, and has shown excellent potential for TDDb analysis. The proposed method shows very good match with experimental data for any type, shape and size of dielectric. In addition, it has the flexibility to model traps formed at any position. It is a physics based close to atomistic simulation model yet does not consume much computational resources. Most importantly it can predict spin current and TMR degradation in MTJ that cannot be done with traditional statistical models.

#### REFERENCES

- [1] Büttiker, M. "Four-Terminal Phase-Coherent Conductance," *Phys. Rev. Lett.*, 57:1761–1764, 1986..
- [2] S. Datta, *Quantum Transport*, 2nd ed. Cambridge, U.K.: Cambridge Univ. Press, 2005.
- [3] H. Kubota, et. al., "Quantitative measurement of voltage dependence of spin-transfer torque in MgO-based magnetic tunnel junctions", *Nat. Phys.*, vol. 4, no. 1, pp. 37-41, 2008.
- [4] M. A. Alam, B. E. Weir, and P. J. Silverman, "A study of soft and hard breakdown -.Part I: Analysis of statistical percolation conductance", *IEEE Trans. Electron Devices*, vol. 49, pp. 232-238, 2002
- [5] B. Weir, C. Leung, P. Silverman, M. A. Alam, "Gate dielectric breakdown in the time-scale of ESD events," *Microelectron. Reliab.* vol.45, pp.427-436, 2005.
- [6] M. A. Alam, B. E. Weir, and P. J. Silverman, "A study of soft and hard breakdown -.Part II: Principles of area, thickness, and voltage scaling", *IEEE Trans. Electron Devices*, vol. 49, pp. 239-246, 2002
- [7] M. A. Alam , B. Weir , J. Bude , P. Silverman and D. Monroe, "Explanation of soft and hard breakdown and its consequences for area scaling", *IEDM Tech. Digest*, pp. 449-452, 1996.
- [8] M. A. Alam, "SILC as a Measure of Trap Generation and Predictor of TBD in Ultrathin Oxides", *IEEE Transaction on Electron Devices*, 49 (2), pp. 226-231, 2002.
- [9] M. A. Alam, B. E. Weir, and P. J. Silverman, "A Study of Soft and Hard Breakdown : The Statistical Model," *IEEE Transaction on Electron Devices*, 49 (2), pp. 232-238, 2002.
- [10] M. Masuduzzaman, A.E. Islam, M.A. Alam, "Exploring the capability of multi-frequency charge pumping in resolving location and energy levels of traps with dielectric", *IEEE Trans Electron Dev*, 55 (12) (2008), pp. 3421–3431
- [11] R. P. Vedula, S. Palit, M. A. Alam, and A. Strachan, "Role of Atomic Variability in Dielectric Charging: A First Principles-based Multi-scale Modeling Study", *Physical Review B*, vol. 88 (20), pp. 2052042013.
- [12] [6] T. Nigam et. al., "Accurate model for time-dependent dielectric breakdown of high- $\kappa$  metal gate stacks," in *Proc. IEEE IRPS*, 2009, pp. 523-530.
- [13] M. Julliere (1975). "Tunneling between ferromagnetic films". *Phys. Lett.* 54A: 225–226.
- [14] Datta, S. *Lessons from Nanoelectronics: A New Perspective on Transport* (World Scientific, 2012).
- [15] D. Datta , B. Behin-Aein , S. Salahuddin and S. Datta, "Quantitative model for TMR and spin-transfer torque in MTJ devices ", *Proc. IEEE Int. Electron Device Meeting*, pp. 22.8.1-22.8.4, Dec. 2010.
- [16] Ahmed Kamal Reza, Xuanyao Fong, Zubair Al Azim, and Kaushik Roy, "Modeling and Evaluation of Topological Insulator/Ferromagnet Heterostructure-Based Memory", *IEEE TRANSACTIONS ON ELECTRON DEVICES*, VOL. 63, NO. 3, MARCH 2016
- [17] R. O'Connor , L. Pantisano and R. Degraeve, "SILC defect generation spectroscopy in HfSiON using constant voltage stress and substrate hot electron injection", *Proc. IEEE IRPS*, pp. 324-329, 2008.
- [18] M. A. Alam, B. Weir, J. Bude, P. Silverman, and D. Monroe, "Explanation of soft and hard breakdown and its consequences for area scaling", *Dig. 1999 Int. Electron Devices Meeting*, pp. 449-452, 1999.
- [19] Kenji Komiya and Yasuhisa Omura, "Aspects of Hard Breakdown Characteristics in a 2.2-nm-thick SiO<sub>2</sub>-Film", *Journal of Semiconductor technology and science*, vol. 2, No. 3, September, 2002
- [20] [Online] ITRS roadmap, <http://www.itrs.net/reports.html>
- [21] M. Haney, R. Nair, and T. Gu, "Chip-scale integrated optical interconnects: a key enabler for future high-performance computing," *Proc. SPIE*, vol 8267, 82670X, Feb. 2012.
- [22] G. Wang et al., "Atomically smooth ultrathin films of topological insulator Sb<sub>2</sub>Te<sub>3</sub>," *Nano Res.*, vol. 3, no. 12, pp. 874–880, 2010.
- [23] C. L. Kane and E. J. Mele, "Z<sub>2</sub> topological order and the quantum spin Hall effect," *Phys. Rev. Lett.*, vol. 95, no. 14, p. 146802, 2005.
- [24] R. Yu, W. Zhang, H.-J. Zhang, S.-C. Zhang, X. Dai, and Z. Fang, "Quantized anomalous Hall effect in magnetic topological insulators," *Science*, vol. 329, no. 5987, pp. 61–64, 2010.
- [25] T. Yokoyama, J. Zang, and N. Nagaosa, "Theoretical study of the dynamics of magnetization on the topological surface," *Phys. Rev. B*, vol. 81, no. 24, p. 241410, 2010.
- [26] Z. Jiang, F. Katmis, C. Tang, P. Wei, J. S. Moodera, and J. Shi, "A comparative transport study of Bi<sub>2</sub>Se<sub>3</sub> and Bi<sub>2</sub>Se<sub>3</sub>/yttrium iron garnet," *Appl. Phys. Lett.*, vol. 104, no. 22, p. 222409, 2014.
- [27] J. Sinova, D. Culcer, Q. Niu, N. A. Sinitsyn, T. Jungwirth, and A. H. MacDonald, "Universal intrinsic spin Hall effect," *Phys. Rev. Lett.*, vol. 92, no. 12, p. 126603, 2004.
- [28] J. M. Luttinger, "The effect of a magnetic field on electrons in a periodic potential," *Phys. Rev. B*, vol. 84, no. 4, pp. 814–817, 1951.
- [29] S. Datta, *Quantum Transport*, 2nd ed. Cambridge, U.K.: Cambridge Univ. Press, 2005.
- [30] C. Augustine, A. Raychowdhury, D. Somasekhar, J. Tschanz, V. De, and K. Roy, "Design space exploration of typical STT MTJ stacks in memory arrays in the presence of variability and disturbances," *IEEE Trans. Electron Devices*, vol. 58, no. 12, pp. 4333–4343, Dec. 2011.
- [31] R. O'Connor, G. Hughes, and P. Casey, "Degradation and breakdown characteristics of thin MgO dielectric layers" *J. Appl. Phys.* 107, 024501, 2010.
- [32] C. Yoshida, et. al., "A study of dielectric breakdown mechanism in CoFeB/MgO/CoFeB magnetic tunnel junction", *Proc. Int. Rel. Phys. Symp. (IRPS)*, pp. 139-142.